



The genome-scale metabolic model iIN800 of *Saccharomyces cerevisiae* and its validation: a scaffold to query lipid metabolism

Nookaew, Intawat; Jewett, Michael Christopher; Meechai, Asawin; Thammarongtham, Chinae; Laoteng, Kobkul; Cheevadhanarak, Supapon; Nielsen, Jens; Bhumiratana, Sakarindr

Published in:
BMC Systems Biology

Link to article, DOI:
[10.1186/1752-0509-2-71](https://doi.org/10.1186/1752-0509-2-71)

Publication date:
2008

Document Version
Publisher's PDF, also known as Version of record

[Link back to DTU Orbit](#)

Citation (APA):
Nookaew, I., Jewett, M. C., Meechai, A., Thammarongtham, C., Laoteng, K., Cheevadhanarak, S., Nielsen, J., & Bhumiratana, S. (2008). The genome-scale metabolic model iIN800 of *Saccharomyces cerevisiae* and its validation: a scaffold to query lipid metabolism. *BMC Systems Biology*, 2, 71. <https://doi.org/10.1186/1752-0509-2-71>

General rights

Copyright and moral rights for the publications made accessible in the public portal are retained by the authors and/or other copyright owners and it is a condition of accessing publications that users recognise and abide by the legal requirements associated with these rights.

- Users may download and print one copy of any publication from the public portal for the purpose of private study or research.
- You may not further distribute the material or use it for any profit-making activity or commercial gain
- You may freely distribute the URL identifying the publication in the public portal

If you believe that this document breaches copyright please contact us providing details, and we will remove access to the work immediately and investigate your claim.

Research article

Open Access

The genome-scale metabolic model *iIN800* of *Saccharomyces cerevisiae* and its validation: a scaffold to query lipid metabolism

Intawat Nookaew¹, Michael C Jewett^{5,6}, Asawin Meechai¹,
Chinae Thammamongtham², Kobkul Laoteng², Supapon Cheevadhanarak³,
Jens Nielsen^{*5,7} and Sakarindr Bhumiratana^{*1,2,4}

Address: ¹Department of Chemical Engineering, Faculty of Engineering, King Mongkut's University of Technology Thonburi, Bangkok 10140, Thailand, ²Biochemical Engineering and Pilot Plant Research and Development Unit, National Center for Genetic Engineering and Biotechnology (BIOTEC) at King Mongkut's University of Technology Thonburi, Bangkok 10150, Thailand, ³School of Bioresources and Technology, King Mongkut's University of Technology Thonburi, Bangkok 10140, Thailand, ⁴National Science and Technology Development Agency, Ministry of Science and Technology, Thailand Science Park, Klong Luang, Pathumthani 12120, Thailand, ⁵Center for Microbial Biotechnology, Biocentrum, Technical University of Denmark, DK-2800 Kgs. Lyngby, Denmark, ⁶Department of Genetics, Harvard Medical School, Boston, MA 02115, USA and ⁷Department of Chemical and Biological Engineering, Chalmers University of Technology, SE-412 96 Gothenburg, Sweden

Email: Intawat Nookaew - intawat.in@gmail.com; Michael C Jewett - mcjewett@genetics.med.harvard.edu; Asawin Meechai - asawin.mee@kmutt.ac.th; Chinae Thammamongtham - chinae@biotec.or.th; Kobkul Laoteng - kobkul@biotec.or.th; Supapon Cheevadhanarak - supapon.che@kmutt.ac.th; Jens Nielsen - nielsenj@chalmers.se ; Sakarindr Bhumiratana* - sakarindr@exchange.nstda.or.th

* Corresponding authors

Published: 7 August 2008

Received: 14 March 2008

BMC Systems Biology 2008, 2:71 doi:10.1186/1752-0509-2-71

Accepted: 7 August 2008

This article is available from: <http://www.biomedcentral.com/1752-0509/2/71>

© 2008 Nookaew et al; licensee BioMed Central Ltd.

This is an Open Access article distributed under the terms of the Creative Commons Attribution License (<http://creativecommons.org/licenses/by/2.0>), which permits unrestricted use, distribution, and reproduction in any medium, provided the original work is properly cited.

Abstract

Background: Up to now, there have been three published versions of a yeast genome-scale metabolic model: *iFF708*, *iND750* and *iLL672*. All three models, however, lack a detailed description of lipid metabolism and thus are unable to be used as integrated scaffolds for gaining insights into lipid metabolism from multilevel omic measurement technologies (e.g. genome-wide mRNA levels). To overcome this limitation, we reconstructed a new version of the *Saccharomyces cerevisiae* genome-scale model, *iIN800* that includes a more rigorous and detailed description of lipid metabolism.

Results: The reconstructed metabolic model comprises 1446 reactions and 1013 metabolites. Beyond incorporating new reactions involved in lipid metabolism, we also present new biomass equations that improve the predictive power of flux balance analysis simulations. Predictions of both growth capability and large scale *in silico* single gene deletions by *iIN800* were consistent with experimental data. In addition, ¹³C-labeling experiments validated the new biomass equations and calculated intracellular fluxes. To demonstrate the applicability of *iIN800*, we show that the model can be used as a scaffold to reveal the regulatory importance of lipid metabolism precursors and intermediates that would have been missed in previous models from transcriptome datasets.

Conclusion: Performing integrated analyses using *iIN800* as a network scaffold is shown to be a valuable tool for elucidating the behavior of complex metabolic networks, particularly for identifying regulatory targets in lipid metabolism that can be used for industrial applications or for understanding lipid disease states.

Background

The yeast *Saccharomyces cerevisiae* is widely used for production of many different commercial compounds such as food, feed, beverages and pharmaceuticals [1]. It also serves as a model eukaryotic organism and has been the subject of more than 40,000 research publications [2,3]. After the complete genome sequence for yeast was released in 1996 [4], about 4,600 ORFs were characterized [3] and yeast contains many genes with human homologs [2]. This has allowed for comparative functional genomics and comparative systems biology between yeast and human. Yeast, for example, has been used to understand the function of complex metabolic pathways that are related to the development of human diseases [5-7].

Several human diseases (e.g. cancer, atherosclerosis, Alzheimer's disease, and Parkinson's disease) are associated with disorders in lipid metabolism [8-10]. The emergence of lipidomics has allowed analysis of lipid metabolism at the systems level [8,11]. Lipidomics promises to make a significant impact in our understanding of lipid related disease development [12]. As with other high-throughput techniques, however, we hypothesize that one of the main challenges for utilization of lipidome data will be our ability to develop appropriate frameworks to integrate and map data for studying relations between lipid metabolism and other cellular networks.

Previous work has shown that genome-scale metabolic models provide an excellent scaffold for integrating data into single, coherent models [13]. The calculation of Reporter Metabolites using genome-scale metabolic models is an example of how metabolic models can be used to upgrade the information content of omics data [14]. This approach allows mapping of key metabolites and reactions in large metabolic networks when combined with transcriptome [14] or metabolome data [15]. However, pathways, reactions, and genes that are not included in the metabolic network cannot be queried. Therefore, the Reporter Metabolite algorithm requires a reliable and global genome scale-model to achieve precise and accurate data interpretation.

So far, three yeast genome-scale metabolic models, *iFF708*, *iND750* and *iLL672*, have been published. All three models, however, lack a detailed description of the lipid metabolism. The first model, *iFF708* [16], consists of 1175 reactions linked to 708 ORFs. *iFF708* shows good predictions of many different cellular functions [17] and gene essentiality predictions [18]. However, almost all intermediate reactions in lipid metabolism were either lumped or neglected. The second model published was *iND750* [19]. *iND750* is fully compartmentalized, consisting of 1498 reactions linked to 750 ORFs. The model was validated by a large-scale gene deletion study and

metabolic phenotypes [20] and was expanded to include regulation for predicting gene expression and phenotypes of different transcription factor mutants [21]. *iND750* contains more reactions and metabolites in lipid metabolism than *iFF708*, but still lacks a comprehensive description of lipid metabolism. The third published model is *iLL672*, which is derived from *iFF708* and comprises 1038 reactions. Several dead-end reactions of *iFF708* were eliminated leading to an improved accuracy of the single gene deletion prediction [22]. However, only minor improvements were made to reactions involved in lipid metabolism. The model was validated using ^{13}C -labeling experiments to study the robustness of different yeast mutants [23].

Here our objective was to expand the genome-scale metabolic model of yeast to include a detailed description of lipid metabolism for use as a scaffold to integrate omics data. We used *iFF708* as a template for building a model based on recent literature that contains new reactions in lipid metabolism and transport relative to all previous models. The new model named *iIN800* includes 92 additional ORFs and provides a more detailed structure of lipid metabolism, tRNA synthesis and transport processes than previous models. The biomass composition, which is very important for flux balance analysis and predicting lethality, was also recalculated and improved. *iIN800* was validated with large-scale gene deletion data and growth simulation predictions. Simulated intracellular fluxes were also supported by ^{13}C -labeling flux experimental data. Finally, we show that the transcriptome data of yeast cultivated under various growth conditions can be integrated with *iIN800* to identify lipid related Reporter Metabolites. We anticipate that *iIN800* will be useful as a scaffold for integrating multilevel omic data and that this new model will have a significant impact in the emerging field of lipidomics.

Results and discussion

Model reconstruction and characteristics of *iIN800*

Due to the complexity of compartmentalization used in *iND750* and the smaller scope of *iLL672*, the metabolic model *iFF708* was selected as a template for the development of the model *iIN800*. Pathway and reaction databases (e.g. KEGG), online resources (e.g. SGD), and literature were used to expand *iFF708*, with particular focus on lipid metabolism. *iIN800* contains 340 total reactions in lipid metabolism, more than at least 143 reactions greater than previous models (Table 1).

To compare metabolic characteristics of the different *in silico* models, lipid metabolism was classified into unique sub-categories (e.g. mitochondrial fatty acid synthesis, ergosterol biosynthesis) (Table 1). Fatty acid synthesis and elongation accounted for three of these sub-catego-

Table 1: Comparison of the number of lipid metabolism reactions among yeast genome-scale metabolic models

Model	<i>iFF708</i>	<i>iLL672</i>	<i>iND750</i>	<i>iIN800</i>
Mitochondrial fatty acid synthesis	14	0	13	45
Cytosolic fatty acid synthesis	17	18	27	48
Fatty acid elongation	0	4	2	33
Fatty acid activation and beta-oxidation	9	19	53	65
Sphingolipid synthesis	18	23	37	27
Phospholipid and TAG synthesis	37	37	35	68
Ergosterol biosynthesis	31	28	30	29
Ergosterol esterification	0	0	0	2
Lipid degradation	0	0	0	23
Total	126	129	197	340

ries. In contrast to previous models, *iIN800* incorporates fatty acid biosynthesis in both mitochondria and the cytosol. Fatty acid synthesis, which involves iterative malonyl-CoA condensations that result in a growing chain of fatty acids, is catalyzed by four major enzymes: β -ketoacyl-ACP synthase (a condensing enzyme), β -ketoacyl-ACP reductase, β -dehydroxyacyl-ACP dehydratase and enoyl-ACP reductase. In the cytosol, these enzymes are encoded by the multifunctional *FAS1* and *FAS2*. In the mitochondria, however, fatty acid synthesis is carried out by the products encoded by *CEM1*, *OAR1*, *HTD2* and *ETR1*. These ORFs were missing from previous models, which prevented simulation of mitochondrial fatty acid synthesis. Fatty acid elongation, which leads to the production of long-chain fatty acids, was not included in *iFF708*, but was also updated in *iIN800*. Including fatty acid elongation resulted in the addition of four major biochemical reaction steps: condensing enzyme, 3-ketoacyl-CoA reductase, enoyl-CoA dehydratase and enoyl-CoA reductase [24]. These reactions are carried out by the enzymes encoded by *ELO1*, *ELO2*, *ELO3*, *IFA38* and *TSC13*. While the gene encoding enoyl-CoA dehydratase has not been identified in *S. cerevisiae*, the reaction was inferred due to the identification of long chain fatty acids in yeast.

β -oxidation is the process where fatty acids, after becoming activated in the form of acyl-CoAs, are broken down to make acetyl-CoA, and ultimately energy. *FAT1*, encoding an enzyme for long-chain fatty acid activation was missing in *iFF708* and *iLL672*. The genes *SPS19*, *ECI1* and *DCI1* are also now included in *iIN800*. As a result, *iIN800* can simulate the oxidation of unsaturated fatty acids.

Sphingolipid synthesis reactions were added to *iIN800* according to a recently reported model [25], resulting in more sphingolipid reactions than the template *iFF708*. Sphingolipid synthesis is the only sub-category in *iIN800* with a significantly lower reaction tally than *iND750*. This is because *iND750* incorporated both C24:0 and C26:0 as very long-chain fatty acids (the back bone of sphingolip-

ids) to produce ceramides. Because the amount of very long chain fatty acids in *S. cerevisiae* is so low relative to other fatty acid species (<2% of total fatty acid pool) [24,26], *iIN800* treats very long chain fatty acids as a single metabolite. As a result, fewer reactions are present in sphingolipid synthesis.

Relative to other models, only minor changes in the biosynthesis of phospholipids and triacylglycerides as well as ergosterol were introduced in *iIN800*. However, esterification of sterols and degradation of lipids, which were not included in all other previous models, are present in *iIN800* (Table 1). Finally, 26 ORFs encoding for tRNA synthesis and one related enzyme, lipoamide dehydrogenase as well as 14 ORFs encoding transporters were also included in *iIN800*. The additionally included ORFs and their related references as well as detailed comparisons of reactions in lipid metabolism of all reported models are given in Additional files 1 and 2, respectively.

In summary, *iIN800* was reconstructed from 17.2% of the characterized ORFs in yeast and contains 1446 metabolic reactions and 1013 metabolites in total. This model is relatively more comprehensive as compared with previously described models (Table 2). The network characteristics of *iIN800* and the starting model *iFF708* are shown in Table 3. Within lipid metabolism, we have incorporated many new reactions in mitochondrial fatty acid synthesis, cytosolic fatty acid synthesis, fatty acid elongation, fatty

Table 2: Structure comparison of *S. cerevisiae* genome-scale metabolic models

Model	Genes	Reactions	Metabolites
<i>iFF708</i>	708(15.2%)*	1175	825
<i>iLL672</i>	672(14.1%)*	1038	636
<i>iND750</i>	750(16.1%)*	1489	972
<i>iIN800</i>	800(17.2%)*	1446	1013

* percentage of associated ORFs in the model relative to characterized ORFs in the yeast genome

Table 3: Network characteristics of the reconstructed metabolic network of *S. cerevisiae* strain *iFF708* and *iIN800*

Model	<i>iFF708</i>	<i>iIN800</i>
Metabolites	825	1013
Cytosolic metabolites	518	631
Mitochondrial metabolites	170	228
Extracellular metabolites	137	154
Reactions	1175	1446
Mitochondrial reactions	104	161
Cytosolic reactions	723	906
Exchange fluxes	348	379
Cytosolic exchange fluxes	286	304
Mitochondrial exchange fluxes	62	75
Reactions with ORF assignments	1075	1209
Biochemical and Physical consideration	140	237

acid activation and β -oxidation, sphingolipid synthesis, ergosterol esterification, and lipid degradation (Table 1). 96 new reactions are derived from biochemical and physical considerations. These reactions mostly describe transportation of fatty acids and lipids across the mitochondria and the plasma membrane. To visualize the model *iIN800*, we constructed a comprehensive metabolic map using ReMapper software (Figure 1). This visualized map provides a method for globally plotting transcript and flux data onto *iIN800*. The source file is available for download (see Methods).

Improved biomass equation

The biomass equation is crucial for using genome-scale models to simulate growth using flux balance analysis (FBA). Therefore, an important consideration in the development of *iIN800* was to address the concern that the biomass composition of *S. cerevisiae* changes under different growth conditions. For example, during growth on excess glucose the carbohydrate content increases and during growth on excess ammonium the protein content increases.

To assess the sensitivity of flux simulations using *iIN800* towards changes in the macro-molecular composition, we performed constraint-based simulations by varying the protein, RNA, carbohydrate and lipid content of the biomass in physiological relevant ranges based on previous experimental reports [27-29], from 35–65%, 3.5–12%, 15–50% and 2–15%, respectively. Specifically, glucose and ammonium uptake rates were minimized for both glucose- and ammonium-limited growth conditions, respectively, using different macromolecular compositions at fixed growth rates, (note: this is the same mathematical problem as fixing uptake rates and maximizing

growth rate). In this way, we could compare the differences between glucose- and ammonium-limited growth conditions. The results are illustrated in Figure 2. An interesting finding was that the protein content strongly affects the uptake rates at both glucose- and ammonium-limited conditions, albeit to a greater extent in ammonium-limited conditions (Fig. 2A). The carbohydrate content on the other hand does not have an impact on the ammonium uptake rate, it strongly impacts the glucose uptake rate (Fig. 2C). The RNA content and the lipid content have only a minor impact on growth (Figures 2B and 2D).

In summary, the sensitivity analysis shows that the biomass composition can significantly impact predictions made with genome-scale metabolic models to varying degrees based on different growth conditions. We therefore present new biomass equations to be used under C-limited and N-limited growth conditions, respectively. These compositions result from previous studies and our own measurements of lipids and fatty acids across multiple N-limited and C-limited growth conditions (data not shown). Using a separate biomass composition for N-limited cultures has not been proposed previously. The N-limited biomass equation is therefore new. Relative to previous C-limited biomass compositions, the most dramatic changes in our here proposed biomass equation is with respect to the lipids and fatty acids (Table 4). While our sensitivity analysis suggests that these components will most likely only lead to a small improvement in the accuracy of C-limited flux simulations, they may play an important role in lethality prediction by the model, as the addition of extra components in the biomass equation will give a higher resolution.

Growth simulation capability

In silico genome-scale models are most generally used to predict various phenotypes. These include growth rates and extracellular secretion rates of metabolite products, as well as uptake rates of nutrients. In addition, models can be employed to explore active route(s) in metabolic pathways under certain growth conditions as illustrated for a genome-scale metabolic model of *E. coli* [30-32] as well as for one of the *S. cerevisiae* genome-scale metabolic models [17].

To validate *iIN800*, we first investigated the model's ability to simulate aerobic and anaerobic growth in glucose- or ammonium-limited conditions. Several published chemostat datasets were used as experimental references. As shown in Figure 3, the results from the computational growth prediction agreed with experimental measurements. Less than 10% relative error was observed (Figure 3). The details of the simulations and the corresponding reference data are given in Additional file 3. Intracellular

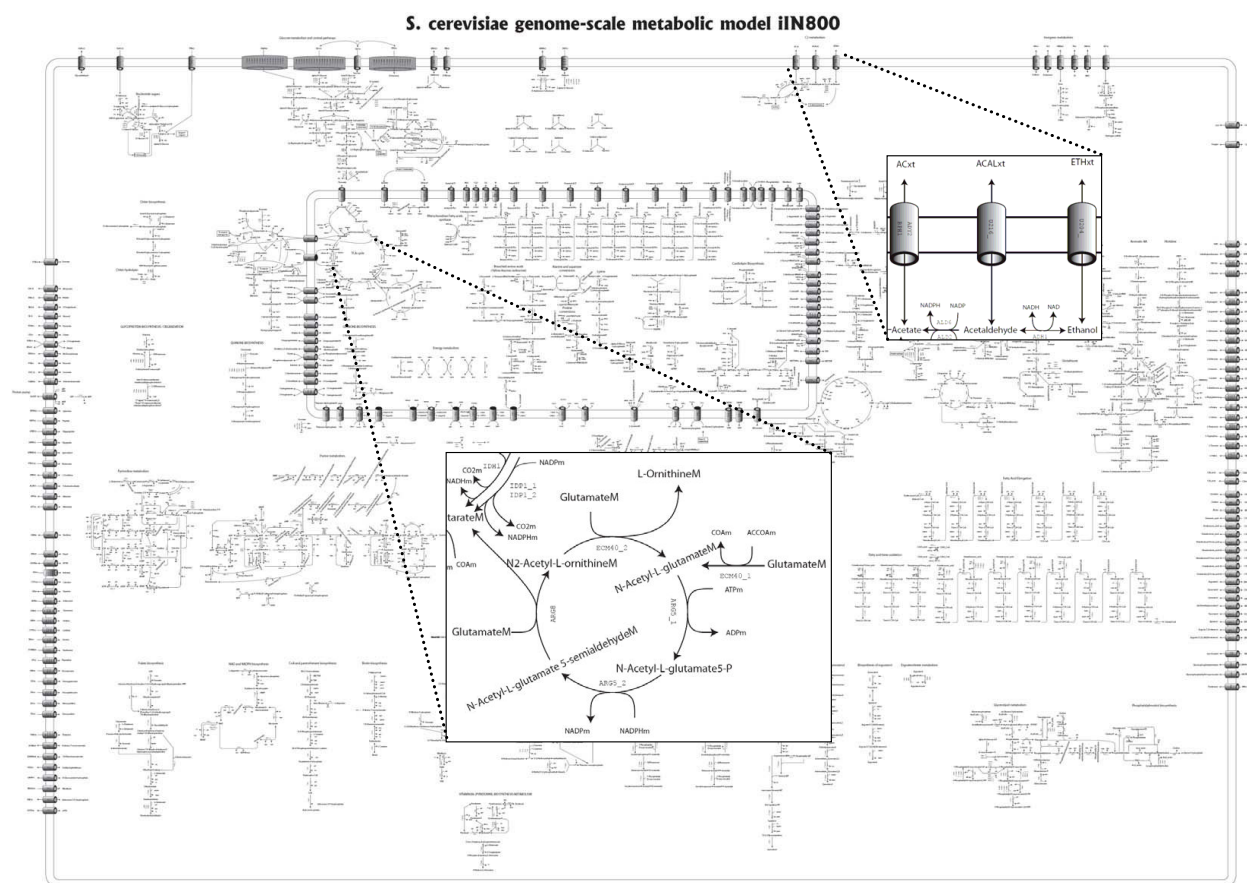


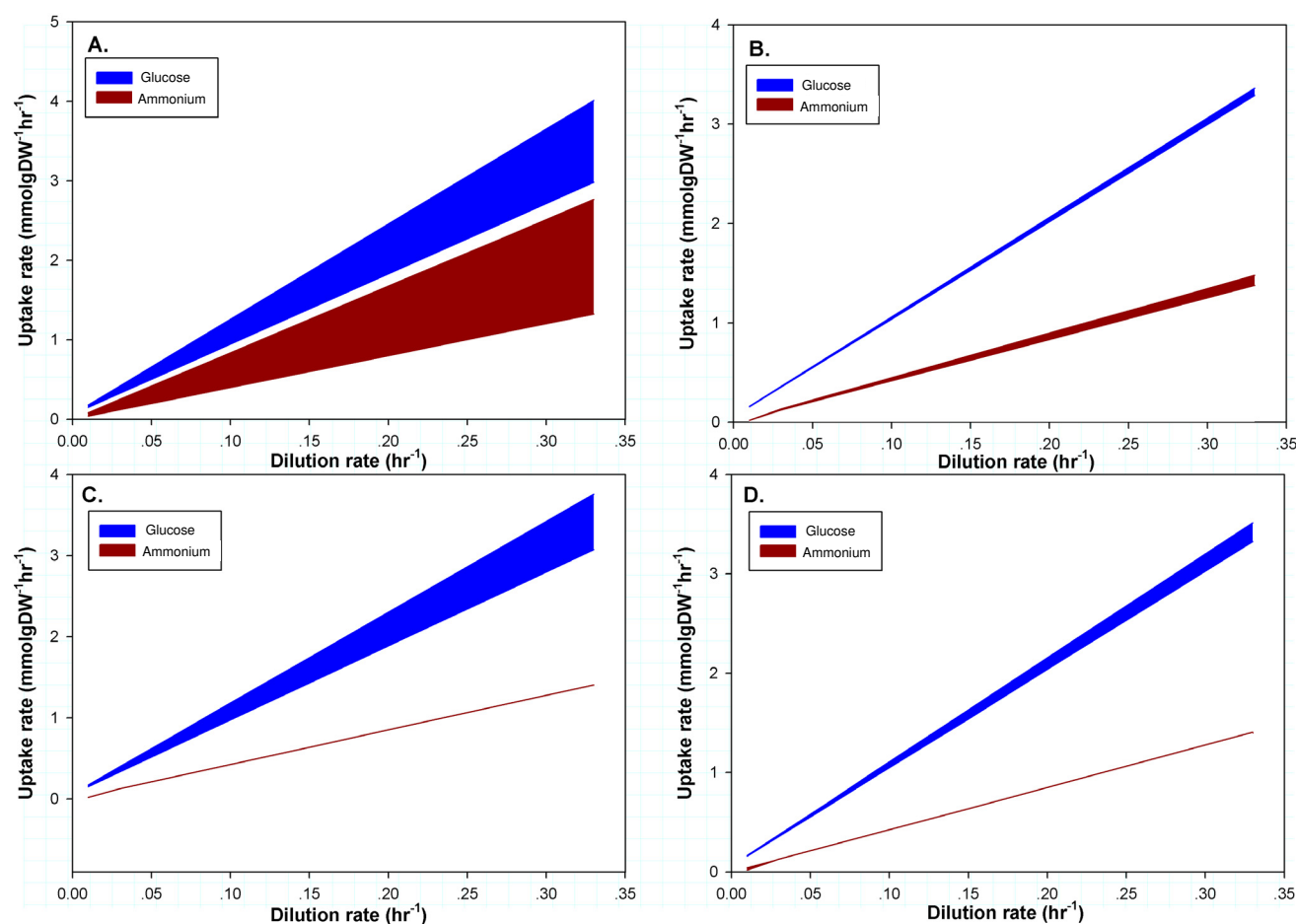
Figure 1
The reconstructed *S. cerevisiae* genome-scale metabolic model iIN800.

fluxes can be easily visualized using the ReMapper software and our model (Additional files 4 and 5).

Since the new biomass equations would be expected to impact the overall flux distributions, we used ^{13}C -flux analysis data to further confirm the computed intracellular fluxes. Specifically, fluxes in the central carbon metabolism at two different growth conditions were both measured by ^{13}C -labeling experiments and calculated by FBA using iIN800. The model validation is shown in Figure 4. There is a high degree of agreement between the predicted and experimental fluxes in the central metabolism, with the exception of fluxes through the pentose phosphate pathway (PPP). Using FBA, the flux through the PPP is largely determined by the requirement for NADPH, and it has earlier been shown difficult to balance NADPH production and consumption [33]. This may explain why the FBA simulations under-predict the flux through this pathway.

Evaluation of large-scale gene deletion

To verify further iIN800, we investigated the ability of the model to predict for growth viability due to a single gene deletion. *In silico* deletion phenotype predictions were examined for the new model with cells grown in both minimal media with a sole carbon source (glucose, galactose, glycerol and ethanol) and with rich media (YPD). iIN800 was assessed for its ability to make correct predictions based on experimental data [22,34]. A summary of the *in silico* single gene deletion predictions are given in Table 5. The overall prediction rate of iIN800, derived from 3392 total predictions, was 89.36%, with 95.50% sensitivity and 38.69% selectivity. The evaluation of the mean of a confusion matrix as the geometric mean of iIN800 equals 60.79%. The performance of the iIN800 model has improved by ~2% and ~7% in terms of overall prediction rate compared with the models iFF708 and iND750, respectively. We believe that the improvement is mainly due to upgrades in the biomass equation, which is

**Figure 2**

Sensitivity analysis shows the influence of macromolecular composition on the simulated growth rate using *iIN800*. The simulations were performed for aerobic glucose- and ammonium-limited cultivations by varying (A) the protein content (35–65%), (B) the RNA content (3.5–12%), (C) the carbohydrate content (15–50%) and (D) the lipid content (2 – 15%).

consistent with results from Kuepfer *et al.* demonstrating that more accurate biomass compositions lead to improved lethality predictions [22]. The false predictions might be due to missing information in gene regulation, biomass compositions, dead-end reactions and medium composition, especially in the rich medium [18,19]

Integration of transcriptome data with genome-scale metabolic models

Genome-scale metabolic models have shown promise for identifying Reporter Metabolites, defined as metabolites whose neighboring genes in a bipartite metabolic graph are most significantly affected and respond as a group to genetic or environmental perturbations [14]. Such an approach has previously been used to reveal important regulatory hot-spots in metabolism from genome-wide expression data and has demonstrated promise for inte-

grating omic data using network topology. To highlight the importance and utility of having a more complete metabolic model in this integrated analysis, the genome-scale models *iIN800* and *iFF708* were used to calculate Reporter Metabolites. Multiple sets of transcriptome data were used for analysis. Lists of the top thirty most significant Reporter Metabolites for several perturbations are compared between *iIN800* and *iFF708* in Table 6, and Reporter Metabolites unique to *iIN800* are marked in bold.

First, transcriptome data from the yeast metabolic cycle [35] were analyzed. Notably, the reporter algorithm identified unique Reporter Metabolites with *iIN800* that would have been missed if *iFF708* was used as the scaffold (Table 6). The most dramatic difference was observed for the reductive charging phase of the metabolic cell cycle.

Table 4: Biomass composition

Metabolites	Amount (mmol/gDW)	
<u>Amino acids</u>	Carbon-limited	Nitrogen-limited
L-Alanine	0.357	0.252
L-Arginine	0.136	0.098
L-Asparagine	0.172	0.153
L-Aspartate	0.172	0.153
L-Cysteine	0.043	0.044
L-Glutamate	0.268	0.231
L-Glutamine	0.268	0.231
Glycine	0.325	0.278
L-Histidine	0.075	0.071
L-Isoleucine	0.172	0.142
L-Leucine	0.250	0.207
L-Lysine	0.239	0.204
L-Methionine	0.050	0.044
L-Phenylalanine	0.114	0.092
L-Proline	0.129	0.118
L-Serine	0.254	0.225
L-Threonine	0.197	0.160
L-Tryptophan	0.027	0.028
L-Tyrosine	0.096	0.068
<u>Carbohydrates</u>	Carbon-limited	Nitrogen-limited
Glycogen	0.519	0.667
alpha,alpha-Trehalose	0.023	0.085
Mannan	0.821	0.994
1,3-beta-D-Glucan	1.136	0.963
<u>RNA</u>	Carbon-limited	Nitrogen-limited
AMP	0.051	0.040
GMP	0.051	0.040
CMP	0.050	0.039
UMP	0.067	0.052
<u>DNA</u>	Carbon-limited	Nitrogen-limited
dAMP	0.004	0.004
dCMP	0.002	0.003
dTMP	0.004	0.004
dGMP	0.002	0.003
<u>Lipids</u>	Carbon-limited	Nitrogen-limited
Phosphatidylcholine	0.002884	0.001660
1-Phosphatidyl-D-myo-inositol	0.001531	0.001656
Phosphatidylserine	0.000373	0.000302
Phosphatidylethanolamine	0.000697	0.000083
Acyl_acids	0.000206	0.000723
Triacylglycerol	0.000781	0.003618
Ergosterol-ester	0.000812	0.004632
Ergosta-5,7,22,24(28)-tetraenol	0.000125	0.000167
Ergosterol	0.005603	0.005155
Zymosterol	0.000015	0.000051
Episterol	0.000096	0.000062
Fecosterol	0.000114	0.000068
Lanosterol	0.000032	0.000074
4,4-Dimethylzymosterol	0.000056	0.000046
Ceramide-I	0.000351	0.000075
Ceramide-II	0.000066	0.000009

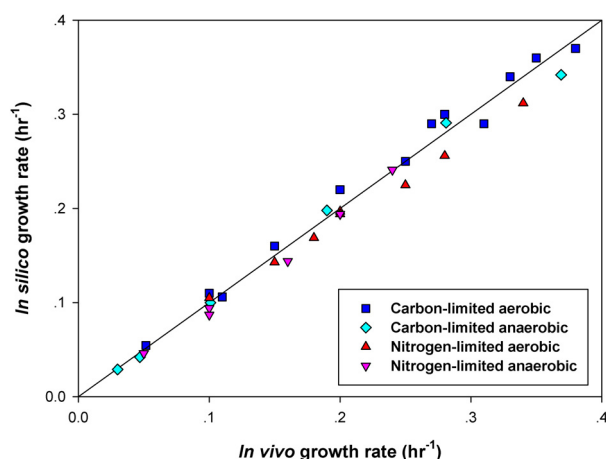


Figure 3
Comparison demonstrating *in silico* and *in vivo* growth rates at various cultivation conditions. *In silico* predictions were performed using FBA with *iIN800*. Experimental measurements were taken from the literature (see text for references).

While both models revealed the importance of regulation controlling the cellular response at glycogen, trehalose, UDP-glucose, glucose-6-P and glucose nodes, only *iIN800* was able to identify key intermediates in β -oxidation. For example, *iIN800* identified *trans*-3-acyl-CoAs, *trans*-2-acyl-CoAs, 3-keto-acyl-CoAs and some fatty acids as Reporter Metabolites (Table 6). This result demonstrates the advantage of expanding the metabolic model to include a much more detailed description of lipid metabolism. Namely, we can now use the genome-scale metabolic model to identify the regulatory importance of lipid precursors and intermediates at different physiological conditions or at different phases of cellular growth. Searching for highly co-regulated subnetworks that implicate lipid genes is also now possible.

Further demonstrations of the applicability of *iIN800* as a scaffold to integrate omic data were performed by analyzing transcriptome data derived from nutrient-limited [36], oxygen-limited [36] and temperature stress conditions [37]. Previously, mRNA and protein levels of genes and enzymes in fatty acid catabolism have been shown to be significantly different between carbon-limited and nitrogen limited growth [38]. When comparing these conditions, only *iIN800* was able to identify fatty acids as Reporter Metabolites (Table 6). In anaerobic yeast cultivation, oleic acid has to be added to the medium because unsaturated fatty acids synthesis is not possible; therefore, the expression of genes in this pathway is induced by the function of the ORE element [39]. Consistent with this

observed cellular response, only *iIN800*, with identified Reporter Metabolites involved in β -oxidation (Table 6). Similarly, *iIN800* was able to highlight the importance of unsaturated fatty acids when comparing high and low temperature cultivations (Table 6), which is known to be important for maintaining proper membrane structure and fluidity [40].

Without the expanded model, the importance of cellular regulation stemming from lipid metabolism would be missed in analyses where metabolic topology is used for integrating data. As an illustration, we integrated results from our Reporter Metabolite analysis with known protein-protein and protein-DNA interaction networks to infer regulatory structure. First, genes associated to Reporter Metabolites in lipid metabolism unique to *iIN800* and determined when comparing carbon- and nitrogen-limited growth (decanoyl-CoA, dodecanoyl-CoA, *trans*-2-C141-CoA, *trans*-2-C161-CoA, *trans*-2-C181-CoA) were identified. These genes were then used to search for highly regulated subnetworks within a protein-protein and protein-DNA interaction network. By applying a p-value threshold of 0.01 to filter for genes with significant gene expression, we inferred a regulatory network controlling the expression of lipid metabolism genes associated to the Reporter Metabolites (Figure 5). Strikingly, regulators at the top of this hierarchy are consistent with those previously known to be significantly changed between carbon- and nitrogen-limited growth. These include: *SNF1*, *SNF4*, *MIG1* and *ADR1* (glucose repression), *OAF1* (β -oxidation), and *INO1* and *INO4* (phospholipid synthesis), among others. Previously reported genome-scale models are not capable of being used as scaffolds for implicating the conditional response of these lipid metabolism regulators because they lack a detailed description of lipid metabolism.

Conclusion

Genome-scale metabolic models have emerged as a valuable tool in the post-genomic era for illustrating whole-cell functions based on the complete network of biochemical reactions. An iterative reconstruction process is required to achieve a comprehensive *S. cerevisiae* genome-scale metabolic model. In this work, we focused on improving the formulation of lipid metabolism relative to previously published *S. cerevisiae* genome-scale metabolic models. Validating the model and new biomass equations, the constraint-based simulation of *iIN800* showed accurate predictions of cellular growth and is also consistent with ^{13}C -labeling experiments. Furthermore, *in silico* gene essentialness predictions were found to be in high agreement with *in vivo* results. Finally, we show that *iIN800*, being more complete, is a better network scaffold for integration of multilevel omics data.

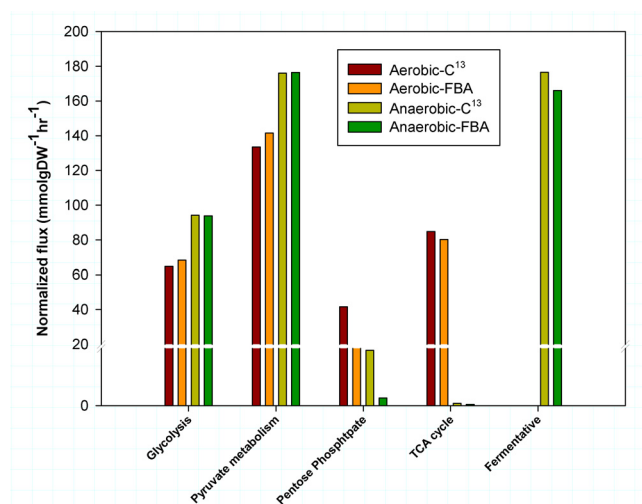


Figure 4
Comparisons of the major intracellular fluxes in the central metabolism calculated using FBA with *iIN800* and ¹³C-labeling metabolic flux analysis at a dilution rate of 0.05 h⁻¹ of either aerobic or anaerobic glucose-limited conditions.

In conclusion, by incorporating a more complete description of lipid metabolism, *iIN800* is positioned to have a broader impact than previously described yeast models. Its capability of predictions were consistent with a number of experimental data both quantitatively (growth rate) and qualitatively (gene essentialness). Moreover, the new model is positioned to be used for studying the regulation and role of lipid metabolism during different growth conditions. With the high degree of homology in lipid metabolism between yeast and humans and emergence of lipidomics, this is expected to allow for new insights into the connection between lipid metabolism and overall cellular function for industrial and medical applications.

Methods

Model reconstruction and visualization

Reconstruction of the *S. cerevisiae* genome-scale metabolic model was done by expanding *iFF708* [16]. The additional ORFs included in the expansion procedure were involved in lipid metabolism, tRNA synthesis and lipoa-mide dehydrogenase. These ORFs were added based on publications listed in Additional file 1. Online resources related to *S. cerevisiae*, such as SGD [41], MIPS [42] and YPD [43], were also used to confirm the existence of the ORFs and their function. Pathway and reaction databases including KEGG [44], ExPASy [45], and Reactome [46], were used together with research papers to identify relevant information of the additional reactions and metabolites, e.g. stoichiometry and co-factor usage. The expanded *iFF708*, called *iIN800*, was visualized by Adobe Illustrator

software (Adobe Systems), and then converted to EPS format (Adobe Systems) format which is downloadable as Additional file 6. In this visualization file, it is possible to overlay information about transcription, fluxes etc. A detailed list of metabolic reactions in *iIN800* is provided as Additional file 7.

Metabolic modeling and simulations

The reaction set in *iIN800* was used for construction of a stoichiometric matrix S ($m \times n$). In the stoichiometric matrix, $m = 1013$, which is the number of metabolites, and $n = 1446$, which is the number of metabolic reactions. With an assumption of steady state for all metabolite pools, a linear equation constraining the fluxes in the metabolic network is obtained [30,47]:

$$S \cdot v = 0 \quad (1)$$

Here v is a vector that contains all the fluxes in the model. Equation (1) has a large number of degrees of freedom, i.e. it is an underdetermined problem, and linear programming was employed to solve the equation system by maximizing an objective function Z (equal to the growth rate), an approach generally referred to as flux balance analysis (FBA) [30,47]. The problem formulation is described below.

Maximize:

$$Z = \omega \cdot v$$

Subject to:

$$S \cdot v = 0$$

$$\alpha \leq v \leq \beta$$

where α and β are lower and upper bounds of fluxes respectively, ω is a weight vector indicating an amount of desired metabolites for biomass synthesis. For irreversible fluxes semi-positive infinite boundary was applied as $0 \leq v \leq \infty$, and fully infinite boundaries was applied as $-\infty \leq v \leq \infty$ for reversible fluxes. The problem was solved by using the commercial linear programming software package LINDO (Lindo systems Inc., Chicago, IL, USA). The calculated intracellular fluxes were overlaid on the visualized genome-scale map as described previously by the ReMapper software (The software has been developed for visualization of multilevel omics data onto a metabolic map.).

Calculation of biomass composition and sensitivity analysis

The biomass composition was re-calculated in order to improve the prediction of the model during growth at different nutrition-limitations, i.e. carbon- and nitrogen-lim-

Table 5: Summary of large-scale single gene deletion evaluation of *S. cerevisiae* *iIN800*.

Evaluation	Glucose*	Glucose**	Minimal media on			Rich media	
			Galactose	Glycerol	Ethanol	YPD	Total
TP	468	469	461	461	463	567	2889
TN	23	23	20	17	21	38	142
FP	37	37	42	45	43	21	225
FN	14	13	19	19	15	56	136
Number of deletions	542	542	542	542	542	682	3392
Positive prediction rate	92.67	92.69	91.65	91.11	91.50	96.43	92.77
Negative prediction rate	62.16	63.89	51.28	47.22	58.33	40.43	51.08
Accuracy	90.59	90.77	88.75	88.19	89.30	88.71	89.36
Sensitivity	97.10	97.30	96.04	96.04	96.86	91.01	95.50
Selectivity	38.33	38.33	32.26	27.42	32.81	64.41	38.69
Geometric mean	61.01	61.07	55.66	51.32	56.38	76.56	60.79

* = Aerobic growth, ** = Anaerobic growth

TP = true positive, TN = true negative, FP = false positive, FN = false negative.

ited growth condition. The contents of macro-molecules were extracted from the thesis of Schulze [27] who measured the biomass composition at a dilution rate of 0.1 h⁻¹. The calculations were performed as described previously [16]. The calculation of protein precursors, i.e. amino acids, and carbohydrate precursors, i.e. trehalose, glycogen, manna and glucan, were adopted from Schulze's work [27]. Deoxyribonucleotide and ribonucleotide compositions were calculated from the study of Vaughan-Martini and co-workers [48]. Lipid compositions were calculated from our own measurements of structural lipidomics, which contains phospholipids, triacylglycerol, sterols, sterol-esters, sphingolipids, free fatty acids and fatty acids composition of all measured lipid classes (unpublished data). The impact of the macromolecular composition on biomass yield was explored in aerobically glucose- and ammonium-limited conditions by fixing the specific growth rate and then minimizing the glucose and ammonium uptake rates at both glucose- and ammonium-limited growth conditions. Four parameters were evaluated, namely the protein, RNA, carbohydrate and lipid content of the biomass.

Growth simulations

The metabolic capabilities of *iIN800* were evaluated by using FBA and linear programming to simulate the biomass flux representing the *in silico* growth rate, which were derived by maximizing the biomass production. Data from various carbon-limited and nitrogen-limited chemostat experiments performed at either aerobic or anaerobic growth condition were taken from the literature for comparisons (see references in Additional file 3). These data were used to validate the metabolic capabilities of the model by comparing *in silico* biomass yields with *in vivo* biomass yields. The *in silico* biomass yields were calculated by fixing measurable uptake rates of extracellular metabolites, such as glucose, ammonium and oxygen, as

well as secretions rates of acetate, glycerol, ethanol, succinate, pyruvate and carbon dioxide. The biomass equation (or flux), which was the objective function, was changed depending on the growth conditions evaluated according to the data provide in Table 4.

Large-scale gene essentiality simulations

The impact of individual gene deletions on cell growth of *iIN800* was evaluated by eliminating the reaction(s) corresponding to each gene in the model from the stoichiometric matrix *S* and then simulating growth of the mutant by FBA. The *in silico* gene essentialities were simulated for growth on rich- and minimal-medium. For minimal media, different carbon sources (glucose, galactose, glycerol and ethanol), ammonium, sulphate and phosphate were evaluated. For rich media, the uptake fluxes of amino acids, purines and pyrimidines were added as additional constraints as previously described [18]. The *in silico* simulations were compared to experimental data available in the MIPS and SGD databases and from competitive growth assays [34] as well as yeast mutant array experiments [22]. The power of *iIN800* to predict gene essentiality was evaluated based on the criteria defined as follows:

$$\text{Accuracy} = (\text{TP} + \text{TN}) / (\text{TP} + \text{TN} + \text{FP} + \text{FN})$$

$$\text{Sensitivity} = \text{TP} / (\text{TP} + \text{FN})$$

$$\text{Specificity} = \text{TN} / (\text{TN} + \text{FP})$$

$$\text{Positive predictive value} = \text{TN} / (\text{TP} + \text{FP})$$

$$\text{Negative predictive value} = \text{TN} / (\text{TN} + \text{FN})$$

$$\text{Geometric mean} = (\text{Sensitivity} \cdot \text{Specificity})^{1/2}$$

Table 6: Top thirty Reporter Metabolites calculated from various perturbations. The Reporter Metabolite algorithm was performed with *iIN800* and *iFF708*.

Oxidative phase ¹		Reductive building phase ¹		Reductive charging Phase ¹	
<i>iIN800</i>	<i>iFF708</i>	<i>iIN800</i>	<i>iFF708</i>	<i>iIN800</i>	<i>iFF708</i>
AMP	IMP	AMPM	AMPM	Dodecanoyl-CoA*	Acyl-CoA
IMP	Xanthosine 5'-phosphate	PyrophosphateM	tRNA ^M	Decanoyl-CoA*	alpha,alpha'-Trehalose
Pyrophosphate	L-Methionine	ATPM	PyrophosphateM	Trans-3-C16-CoA*	Glycogen
L-Methionine	5-Phospho-alpha-D-ribose 1-PP	tRNA ^M	Porphobilinogen	Trans-3-C18-CoA*	alpha,alpha'-Trehalose 6-phosphate
Xanthosine 5'-phosphate	L-Aspartate	H+M	L-TryptophanM	Trans-3-C14-CoA*	alpha-D-Glucose
ATP	Sulfate	NADHM	L-Tryptophanyl-tRNA(Trp)M	alpha,alpha'-Trehalose	Oxalosuccinate
5-Phospho-alpha-D-ribose 1-PP	Homocysteine	Porphobilinogen	Dolichyl beta-D-mannosyl-P	Glycogen	3-Oxoacyl-CoA
L-Serine	AMP	Dolichyl beta-D-mannosyl-P	Mannan	alpha,alpha'-Trehalose 6-phosphate	a Long-chain carboxylic acid
L-Aspartate	H+EXT	L-Tryptophanyl-tRNA(Trp)M	Xanthine	Oxalosuccinate	Carnitine
H+EXT	3-Phosphonooxypyruvate	Mannan	L-AsparaginyI-tRNA(Asn)M	Trans-2-C14-CoA*	alpha-D-Glucose 6-phosphate
Homocysteine	N6-(L-1,3-Dicarboxypropyl)-L-lysine	tRNA(Ile)M*	H+M	Trans-2-C16-CoA*	UDPglucose
Sulfate	5,10-Methylenetetrahydrofolate	L-Isoleucyl-tRNA(Ile)M*	Dolichyl phosphate	Trans-2-C18-CoA*	Isocitrate
L-Glutamine	Aminoimidazole ribotide	tRNA(Thr)M*	all-trans-Nonaprenyl-PP	3-keto-Dodecanoyl-CoA*	D-Glucose 1-phosphate
L-Cysteine	L-Cystathionine	L-Threonyl-tRNA(Thr)M*	NADHM	3-keto-Decanoyl-CoA*	CoAM
L-Asparagine	L-Serine	Xanthine	ATPM	3-keto-Octanoyl-CoA*	Acetyl-CoAM
S-Adenosyl-L-methionine	Uracil	Dolichyl phosphate	D-Mannose 6-phosphate	3-keto-Hexanoyl-CoA*	CoA
Uracil	Sulfite	all-trans-Nonaprenyl-PP	UbiquinolM	3-keto-Butanoyl-CoA*	O-Acetylcarnitine
5,10-Methylenetetrahydrofolate	5-amino-4-imidazolecarboxylate	L-AsparaginyI-tRNA(Asn)M	Ubiquinone-9M	Dodecanoic_acid*	Succinate
3-Phosphonooxypyruvate	2-Hydroxybutane-1,2,4-tricarboxylate	tRNA(Phe)M*	CO2M	Carnitine	(S)-3-Hydroxy-3-methylglutaryl-CoA
N6-(L-1,3-Dicarboxypropyl)-L-lysine	S-Adenosyl-L-methionine	L-Phenylalanyl-tRNA(Phe)M*	Guanosine	alpha-D-Glucose	NAD+
L-Cystathionine	L-Asparagine	Intermediate_Methylzymosterol_II	IsocitrateM	Trans-2-4-diene-CoA*	H2O2
NH3	5-Phosphoribosylamine	Intermediate_Zymosterol_II	GTPM	Isocitrate	Malate
tRNA(Phe)*	GlycineM	UbiquinolM	GDPM	alpha-D-Glucose 6-phosphate	Maltose
L-Phenylalanyl-tRNA(Phe)*	Guanine	D-Mannose 6-phosphate	ITPM	UDPglucose	(3S)-3-Hydroxyacyl-CoA
Tetrahydrofolate	L-Histidine	Ubiquinone-9M	IDPM	D-Glucose 1-phosphate	GLCxt
Guanine	N1-(5'-phosphoribosyl)acetamidine	tRNA(Asp)M*	ITP	O-Acetylcarnitine	Glycerone phosphate
Sulfite	Tetrahydrofolate	L-Aspartyl-tRNA(Asp)M*	IDP	Tetradecanoyl-CoA*	O-AcetylcarnitineM
L-Histidine	alpha-D-Glutamyl phosphate	tRNA(Pro)M*	Phosphatidate	Decanoic_acid*	CarnitineM
5-amino-4-imidazolecarboxylate	HomoisocitrateM	L-Prolinyl-tRNA(Pro)M*	C100ACPM	(S)-3-Hydroxy-3-methylglutaryl-CoA	D-Galactose
GlycineM	GMP	Pyrophosphate	Dodecanoyl-ACPM	H2O2	SuccinateM

* Metabolite is contained in *iIN800* only

1 = data from Tu, B. P., A. Kudlicki, et al. (2005)

Table 6: Top thirty Reporter Metabolites calculated from various perturbations. The Reporter Metabolite algorithm was performed with *iIN800* and *iff708*. (Continued)

Carbon- and Nitrogen-limited ²		Aerobic and Anaerobic ²		Temperature(30°C and 15°C) ³	
<i>iIN800</i>	<i>iff708</i>	<i>iIN800</i>	<i>iff708</i>	<i>iIN800</i>	<i>iff708</i>
Glyoxylate	Glyoxylate	Oxygen	Ferricytochrome cM	IMP	IMP
GLUxt	L-Phenylalanine	Ferricytochrome cM	Ferrocyclochrome cM	Tetrahydrofolate	Tetrahydrofolate
Isocitrate	GLUxt	Ferrocyclochrome cM	Ubiquinone-9M	alpha,alpha-Trehalose	alpha,alpha-Trehalose
ALAxt	Isocitrate	Ubiquinone-9M	Oxygen	Hexadecanoyl-9-ene-CoA*	D-Erythrose 4-phosphate
Malate	ALAxt	UbiquinolM	UbiquinolM	Octadecanoyl-9-ene-CoA*	L-OrnithineM
Allantoate	Allantoate	ADPM	ADPM	Tetradecanoyl-9-ene-CoA*	Xanthosine 5'-phosphate
SERxt	Malate	H+M	H+M	D-Erythrose 4-phosphate	N6-(L-1,3-Dicarboxypropyl)-L-lysine
L-Alanine	L-Alanine	Dodecanoyl-CoA*	FADH2M	L-OrnithineM	NADH
Decanoyl-CoA*	SERxt	FumarateM	FumarateM	Xanthosine 5'-phosphate	URLxt
ASNxt	ASNxt	OrthophosphateM	OrthophosphateM	N6-(L-1,3-Dicarboxypropyl)-L-lysine	1-Phosphatidyl-D-myo-inositol 4-P
GLNxt	GLNxt	FADH2M	Sphinganine 1-phosphate	URLxt	Homocysteine
ILExt	ILExt	Hexadecanoyl-9-ene-CoA*	ATPM	Homocysteine	1-Phosphatidyl-D-myo-inositol 4,5-PP
VALxt	VALxt	Octadecanoyl-9-ene-CoA*	Fumarate	Octadecanoyl-CoA	N-Acetyl-L-glutamateM
Trans-2-C161-CoA*	Ferricytochrome cM	Tetradecanoyl-9-ene-CoA*	Glyoxylate	N-Acetyl-L-glutamateM	Dihydrofolate
Trans-2-C181-CoA*	Ferrocyclochrome cM	Sphinganine 1-phosphate	Isocitrate	Dihydrofolate	N2-Acetyl-L-ornithineM
Trans-2-C141-CoA*	PHExt	Phytosphingosine 1-phosphate	ERGOSTxt	N2-Acetyl-L-ornithineM	Anthranilate
PHExt	L-Asparagine	Tetradecanoyl-Co	ZYMSTxt	Anthranilate	S-Adenosyl-L-homocysteine
Ferricytochrome cM	Allantoin	Fumarate	NAD+	Hexadecanoyl-9-ene_acid*	UREAxt
Ferrocyclochrome cM	LEUxt	Trans-2-C161-CoA*	FADM	Octadecanoyl-9-ene_acid*	L-Aspartate
FRUxt	FRUxt	Trans-2-C181-CoA*	6-Phospho-D-gluconate	S-Adenosyl-L-homocysteine	N(pai)-Methyl-L-histidine
Allantoin	Succinate	Trans-2-C141-CoA*	1,3-Diaminopropane	NADH	Adenosine 3',5'-bisphosphate
LEUxt	HISxt	Glyoxylate	sn-Glycerol 3-phosphate	UREAxt	4-imidazolecarboxylate
Succinate	TYRxt	sn-Glycerol 3-phosphate	O-Acetylcarnitine	L-Aspartate	3-Methyl-2-oxobutanoateM
HISxt	METxt	Isocitrate	Ethanol	1-Phosphatidyl-D-myo-inositol-3-P	Tetrahydrofolyl-[Glu](n)
Dodecanoyl-CoA*	GLYxt	ERGOSTxt	DIPEPxt	N(pai)-Methyl-L-histidine	2-Phenylacetamide
PROxt	ASPxt	ZYMSTxt	Dipeptide	Adenosine 3',5'-bisphosphate	Phenylacetic acid
alpha-D-Mannose	GLCxt	1,3-Diaminopropane	OPEPxt	L-Asparagine	Indole-3-acetamide
Trans-3-C16-CoA*	L-Tyrosine	6-Phospho-D-gluconate	Oligopeptide	C24-CoA*	Indole-3-acetate
Trans-3-C18-CoA*	PROxt	H2O2	PEPTxt	1-(5-Phospho-D-ribosyl)-5-amino	Urea-1-carboxylate
Trans-3-C14-CoA*	alpha-D-Mannose	Trans-3-C16-CoA*	Sphinganine	3-Methyl-2-oxobutanoateM	PhosphatidylserineM

* Metabolite is contained in *iIN800* only

2 = Tai, S. L., V. M. Boer, et al. (2005)

3 = Pizarro, F., M.C. Jewett, et al. (2008)

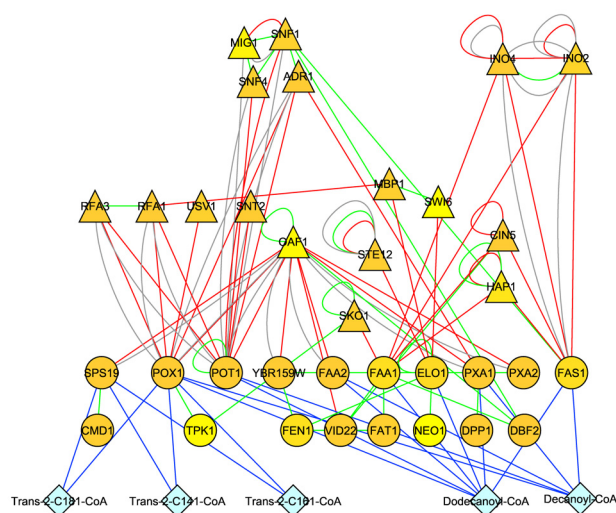


Figure 5
Regulatory module implicated in the control of lipid metabolism genes associated to *iIN800* Reporter Metabolites, which were determined by comparing N-limited and C-limited growth. Without the expanded model *iIN800*, the importance of cellular regulation stemming from lipid metabolism would be missed. High scoring Reporter Metabolites (diamonds), metabolic genes associated to Reporter Metabolites (circles), and genes encoding regulators (triangles). The blue, red, gray and green edges represent metabolite-gene interactions from the genome-scale metabolic model, protein-DNA interactions from ChIP-CHIP data, protein-DNA interactions from YPD and protein-protein interactions from BioGRID, respectively.

where TP = true positive, TN = true negative, FP = false positive, FN = false negative. Positive and negative values referred to viable and lethal phenotype, respectively.

Reporter Metabolite determination

Published microarray data were retrieved from Gene Expression Omnibus (GEO) [49]. The CEL files were normalized by the dChip software [50] in order to minimize overall intensity variation among a set of chips. The statistical test of significance was done by ANOVA or student t-test for p-value calculation.

Briefly, we describe the Reporter Metabolite calculations. The genome-scale model was converted to a bipartite undirected graph. In this graph each metabolite node has as neighbors the enzymes catalyzing the formation and consumption of the metabolite. The transcriptome data were mapped on the enzyme nodes using the significant values of gene expression. The normal commutative distribution was used to convert the p-values to a Z-score for further calculations. To identify an importance of metabolites in the metabolic network of the particular experi-

mental conditions, the reporter algorithm was applied as described earlier [14].

Inferring regulatory modules from Reporter Metabolites

The interactome network was initially constructed with data obtained from YPD [43], ChIP-chip databases [51] (protein-DNA interaction) and BioGRID [52] (protein-protein interaction). The candidate genes of high scoring Reporter Metabolites were retrieved from the bipartite metabolite-gene encoding enzyme interaction graph. They were then used to identify subnetworks from the interactome network [53]. Significantly changing p-values from microarray data were mapped on the subnetwork and then also genes having a p-value < 0.01 directly connected with the Reporter Metabolites. The module was visualized by Cytoscape software [54].

Authors' contributions

IN designed the study, performed the metabolic reconstruction and validation, and contributed to manuscript writing. MCJ carried out the C^{13} -labeling flux experiments, helped curate the model and contributed to manuscript writing. AM, CT, KL and SC contributed to the manuscript preparations, JN and SB participated in the concept and design of the study. All authors read and approved the final manuscript.

Additional material

Additional file 1

Additional ORFs. List of additional ORFs and their references containing in *iIN800*.

Click here for file

[<http://www.biomedcentral.com/content/supplementary/1752-0509-2-71-S1.pdf>]

Additional file 2

Lipid metabolism reactions and comparison. Comparison of lipid metabolism reactions of all *S. cerevisiae* genome-scale models.

Click here for file

[<http://www.biomedcentral.com/content/supplementary/1752-0509-2-71-S2.zip>]

Additional file 3

Growth simulation results. Growth simulations and comparison with experimental measurements.

Click here for file

[<http://www.biomedcentral.com/content/supplementary/1752-0509-2-71-S3.pdf>]

Additional file 4

Aerobic Flux distribution. Visualization of flux distribution of aerobic growth mapping on Figure 1.

Click here for file

[<http://www.biomedcentral.com/content/supplementary/1752-0509-2-71-S4.pdf>]

Additional file 5

Anaerobic Flux distribution. Visualization of flux distribution of anaerobic growth mapping on Figure 1.

Click here for file

[<http://www.biomedcentral.com/content/supplementary/1752-0509-2-71-S5.pdf>]

Additional file 6

High resolution file of Figure 1. High resolution of *S. cerevisiae* metabolic map is provided as EPS format.

Click here for file

[<http://www.biomedcentral.com/content/supplementary/1752-0509-2-71-S6.eps>]

Additional file 7

iIN800 model. List of all participated reactions in iIN800 model.

Click here for file

[<http://www.biomedcentral.com/content/supplementary/1752-0509-2-71-S7.pdf>]

Acknowledgements

The authors gratefully thank Mikael Rørdam Andersen and Kiran Raosaheb Patil for providing the ReMapper and the Reporter software, respectively. This work is supported by a grant from the National Center for Genetic Engineering and Biotechnology (BIOTEC) (grant number BT-B-06-NG-B5-4602). Intawat Nookaew gratefully acknowledges financial support by Thai Graduate Student Institute Science and Technology (TGIST). Michael C. Jewett is grateful to the NSF International Research Fellowship Program for supporting his work.

References

- Nielsen J, Jewett MC: **Impact of systems biology on metabolic engineering of *Saccharomyces cerevisiae*.** *FEMS Yeast Res* 2007.
- Botstein D, Chervitz SA, Cherry JM: **Yeast as a model organism.** *Science* 1997, **277**(5330):1259-1260.
- Pena-Castillo L, Hughes TR: **Why are there still over 1000 uncharacterized yeast genes?** *Genetics* 2007, **176**(1):7-14.
- Goffeau A, Barrell BG, Bussey H, Davis RW, Dujon B, Feldmann H, Galibert F, Hoheisel JD, Jacq C, Johnston M, Louis EJ, Mewes HW, Murakami Y, Philippsen P, Tettelin H, Oliver SG: **Life with 6000 genes.** *Science* 1996, **274**(5287):546-563.
- Bassett DE Jr., Boguski MS, Hieter P: **Yeast genes and human disease.** *Nature* 1996, **379**(6566):589-590.
- Foury F: **Human genetic diseases: a cross-talk between man and yeast.** *Gene* 1997, **195**(1):1-10.
- Steinmetz LM, Scharfe C, Deutschbauer AM, Mokranjac D, Herman ZS, Jones T, Chu AM, Giaever G, Prokisch H, Oefner PJ, Davis RW: **Systematic screen for human disease genes in yeast.** *Nat Genet* 2002, **31**(4):400-404.
- German JB, Gillies LA, Smilowitz JT, Zivkovic AM, Watkins SM: **Lipidomics and lipid profiling in metabolomics.** *Curr Opin Lipidol* 2007, **18**(1):66-71.
- Vigh L, Escriba PV, Sonnleitner A, Sonnleitner M, Piotto S, Maresca B, Horvath I, Harwood JL: **The significance of lipid composition for membrane activity: new concepts and ways of assessing function.** *Prog Lipid Res* 2005, **44**(5):303-344.
- Scherzer CR, Feany MB: **Yeast genetics targets lipids in Parkinson's disease.** *Trends Genet* 2004, **20**(7):273-277.
- Mutch DM, Fauconnot L, Grigorenko M, Fay LB: **Putting the 'Ome' in lipid metabolism.** *Biotechnol Annu Rev* 2006, **12**:67-84.
- Gaspar ML, Aregullin MA, Jesch SA, Nunez LR, Villa-Garcia M, Henry SA: **The emergence of yeast lipidomics.** *Biochim Biophys Acta* 2007, **1771**(3):241-254.
- Patil KR, Akesson M, Nielsen J: **Use of genome-scale microbial models for metabolic engineering.** *Curr Opin Biotechnol* 2004, **15**(1):64-69.
- Patil KR, Nielsen J: **Uncovering transcriptional regulation of metabolism by using metabolic network topology.** *Proc Natl Acad Sci U S A* 2005, **102**(8):2685-2689.
- Cakir T, Patil KR, Onsan Z, Ulgen KO, Kirdar B, Nielsen J: **Integration of metabolome data with metabolic networks reveals reporter reactions.** *Mol Syst Biol* 2006, **2**:50.
- Forster J, Famili I, Fu P, Palsson BO, Nielsen J: **Genome-scale reconstruction of the *Saccharomyces cerevisiae* metabolic network.** *Genome Res* 2003, **13**(2):244-253.
- Famili I, Forster J, Nielsen J, Palsson BO: ***Saccharomyces cerevisiae* phenotypes can be predicted by using constraint-based analysis of a genome-scale reconstructed metabolic network.** *Proc Natl Acad Sci U S A* 2003, **100**(23):13134-13139.
- Forster J, Famili I, Palsson BO, Nielsen J: **Large-scale evaluation of in silico gene deletions in *Saccharomyces cerevisiae*.** *Omic* 2003, **7**(2):193-202.
- Duarte NC, Herrgard MJ, Palsson BO: **Reconstruction and validation of *Saccharomyces cerevisiae* iND750, a fully compartmentalized genome-scale metabolic model.** *Genome Res* 2004, **14**(7):1298-1309.
- Duarte NC, Palsson BO, Fu P: **Integrated analysis of metabolic phenotypes in *Saccharomyces cerevisiae*.** *BMC Genomics* 2004, **5**(1):63.
- Herrgard MJ, Lee BS, Portnoy V, Palsson BO: **Integrated analysis of regulatory and metabolic networks reveals novel regulatory mechanisms in *Saccharomyces cerevisiae*.** *Genome Res* 2006, **16**(5):627-635.
- Kuepfer L, Sauer U, Blank LM: **Metabolic functions of duplicate genes in *Saccharomyces cerevisiae*.** *Genome Res* 2005, **15**(10):1421-1430.
- Blank LM, Kuepfer L, Sauer U: **Large-scale ¹³C-flux analysis reveals mechanistic principles of metabolic network robustness to null mutations in yeast.** *Genome Biol* 2005, **6**(6):R49.
- Han G, Gable K, Kohlwein SD, Beaudoin F, Napier JA, Dunn TM: **The *Saccharomyces cerevisiae* YBR159w gene encodes the 3-ketoreductase of the microsomal fatty acid elongase.** *J Biol Chem* 2002, **277**(38):35440-35449.
- Alvarez-Vasquez F, Sims KJ, Cowart LA, Okamoto Y, Voit EO, Hannun YA: **Simulation and validation of modelled sphingolipid metabolism in *Saccharomyces cerevisiae*.** *Nature* 2005, **433**(7024):425-430.
- Welch JW, Burlingame AL: **Very long-chain fatty acids in yeast.** *J Bacteriol* 1973, **115**(1):464-466.
- Schulze U: **Anaerobic physiology of *Saccharomyces cerevisiae*.** Lyngby, Technical University of Denmark; 1995.
- Dyer JM, Chapital DC, Kuan JW, Mullen RT, Pepperman AB: **Metabolic engineering of *Saccharomyces cerevisiae* for production of novel lipid compounds.** *Appl Microbiol Biotechnol* 2002, **59**(2-3):224-230.
- Jollow D, Kellerman GM, Linnane AW: **The biogenesis of mitochondria. 3. The lipid composition of aerobically and anaerobically grown *Saccharomyces cerevisiae* as related to the membrane systems of the cells.** *J Cell Biol* 1968, **37**(2):221-230.
- Edwards JS, Ibarra RU, Palsson BO: **In silico predictions of *Escherichia coli* metabolic capabilities are consistent with experimental data.** *Nat Biotechnol* 2001, **19**(2):125-130.
- Feist AM, Henry CS, Reed JL, Krummenacker M, Joyce AR, Karp PD, Broadbelt LJ, Hatzimanikatis V, Palsson BO: **A genome-scale metabolic reconstruction for *Escherichia coli* K-12 MG1655 that accounts for 1260 ORFs and thermodynamic information.** *Mol Syst Biol* 2007, **3**:121.
- Reed JL, Vo TD, Schilling CH, Palsson BO: **An expanded genome-scale model of *Escherichia coli* K-12 (iJR904 GSM/GPR).** *Genome Biol* 2003, **4**(9):R54.
- Gombert AK, Moreira dos Santos M, Christensen B, Nielsen J: **Network identification and flux quantification in the central metabolism of *Saccharomyces cerevisiae* under different conditions of glucose repression.** *J Bacteriol* 2001, **183**(4):1441-1451.
- Winzler EA, Shoemaker DD, Astromoff A, Liang H, Anderson K, Andre B, Bangham R, Benito R, Boeke JD, Bussey H, Chu AM, Connelly C, Davis K, Dietrich F, Dow SW, El Bakkoury M, Foury F, Friend SH, Gentulén E, Giaever G, Hegemann JH, Jones T, Laub M, Liao H, Liebundguth N, Lockhart DJ, Lucau-Danila A, Lussier M, M'Rabet N,

- Menard P, Mittmann M, Pai C, Rebischung C, Revuelta JL, Riles L, Roberts CJ, Ross-MacDonald P, Scherens B, Snyder M, Sookhai-Mahadeo S, Storms RK, Veronneau S, Voet M, Volckaert G, Ward TR, Wysocki R, Yen GS, Yu K, Zimmermann K, Philippsen P, Johnston M, Davis RW: **Functional characterization of the *S. cerevisiae* genome by gene deletion and parallel analysis.** *Science* 1999, **285**(5429):901-906.
35. Tu BP, Kudlicki A, Rowicka M, McKnight SL: **Logic of the yeast metabolic cycle: temporal compartmentalization of cellular processes.** *Science* 2005, **310**(5751):1152-1158.
 36. Tai SL, Boer VM, Daran-Lapujade P, Walsh MC, de Winde JH, Daran JM, Pronk JT: **Two-dimensional transcriptome analysis in chemostat cultures. Combinatorial effects of oxygen availability and macronutrient limitation in *Saccharomyces cerevisiae*.** *J Biol Chem* 2005, **280**(1):437-447.
 37. Pizarro F, Jewett MC, Nielsen J, Agosin E: **Physiological and transcriptional mapping of evolutionary differences between laboratory and commercial *Saccharomyces cerevisiae* strains(submitted).** 2008.
 38. Kolkman A, Daran-Lapujade P, Fullaondo A, Olsthoorn MM, Pronk JT, Slijper M, Heck AJ: **Proteome analysis of yeast response to various nutrient limitations.** *Mol Syst Biol* 2006, **2**:2006 0026.
 39. Gurvitz A, Mursula AM, Firzinger A, Hamilton B, Kilpelainen SH, Hartig A, Ruis H, Hiltunen JK, Rottensteiner H: **Peroxisomal Delta3-cis-Delta2-trans-enoyl-CoA isomerase encoded by *ECI1* is required for growth of the yeast *Saccharomyces cerevisiae* on unsaturated fatty acids.** *J Biol Chem* 1998, **273**(47):31366-31374.
 40. Rodriguez-Vargas S, Sanchez-Garcia A, Martinez-Rivas JM, Prieto JA, Rande-Gil F: **Fluidization of membrane lipids enhances the tolerance of *Saccharomyces cerevisiae* to freezing and salt stress.** *Appl Environ Microbiol* 2007, **73**(1):110-116.
 41. Hirschman JE, Balakrishnan R, Christie KR, Costanzo MC, Dwight SS, Engel SR, Fisk DG, Hong EL, Livstone MS, Nash R, Park J, Oughtred R, Skrzypek M, Starr B, Theesfeld CL, Williams J, Andrada R, Binkley G, Dong Q, Lane C, Miyasato S, Sethuraman A, Schroeder M, Thanawala MK, Weng S, Dolinski K, Botstein D, Cherry JM: **Genome Snapshot: a new resource at the *Saccharomyces* Genome Database (SGD) presenting an overview of the *Saccharomyces cerevisiae* genome.** *Nucleic Acids Res* 2006, **34**(Database issue):D442-5.
 42. Guldener U, Munsterkotter M, Kastenmuller G, Strack N, van Helden J, Lemer C, Richeltes J, Wodak SJ, Garcia-Martinez J, Perez-Ortin JE, Michael H, Kaps A, Talla E, Dujon B, Andre B, Souciet JL, De Montigny J, Bon E, Gaillardin C, Mewes HW: **CYGD: the Comprehensive Yeast Genome Database.** *Nucleic Acids Res* 2005, **33**(Database issue):D364-8.
 43. Csank C, Costanzo MC, Hirschman J, Hodges P, Kranz JE, Mangan M, O'Neill K, Robertson LS, Skrzypek MS, Brooks J, Garrels JL: **Three yeast proteome databases: YPD, PombePD, and CalPD (MycoPathPD).** *Methods Enzymol* 2002, **350**:347-373.
 44. Arakawa K, Kono N, Yamada Y, Mori H, Tomita M: **KEGG-based pathway visualization tool for complex omics data.** *In Silico Biol* 2005, **5**(4):419-423.
 45. Gasteiger E, Gattiker A, Hoogland C, Ivanyi I, Appel RD, Bairoch A: **ExPASy: The proteomics server for in-depth protein knowledge and analysis.** *Nucleic Acids Res* 2003, **31**(13):3784-3788.
 46. Vastrik I, D'Eustachio P, Schmidt E, Joshi-Tope G, Gopinath G, Croft D, de Bono B, Gillespie M, Jassal B, Lewis S, Matthews L, Wu G, Birney E, Stein L: **Reactome: a knowledge base of biologic pathways and processes.** *Genome Biol* 2007, **8**(3):R39.
 47. Edwards JS, Palsson BO: **The *Escherichia coli* MGI655 in silico metabolic genotype: its definition, characteristics, and capabilities.** *Proc Natl Acad Sci U S A* 2000, **97**(10):5528-5533.
 48. Vaughan-Martini A, Martini A, Cardinali G: **Electrophoretic karyotyping as a taxonomic tool in the genus *Saccharomyces*.** *Antonie Van Leeuwenhoek* 1993, **63**(2):145-156.
 49. Barrett T, Edgar R: **Gene expression omnibus: microarray data storage, submission, retrieval, and analysis.** *Methods Enzymol* 2006, **411**:352-369.
 50. Schadt EE, Li C, Ellis B, Wong WH: **Feature extraction and normalization algorithms for high-density oligonucleotide gene expression array data.** *J Cell Biochem Suppl* 2001, **Suppl 37**:120-125.
 51. Harbison CT, Gordon DB, Lee TI, Rinaldi NJ, Macisaac KD, Danford TW, Hannett NM, Tagne JB, Reynolds DB, Yoo J, Jennings EG, Zeitlinger J, Pokholok DK, Kellis M, Rolfe PA, Takusagawa KT, Lander ES, Gifford DK, Fraenkel E, Young RA: **Transcriptional regulatory code of a eukaryotic genome.** *Nature* 2004, **431**(7004):99-104.
 52. Stark C, Breitkreutz BJ, Reguly T, Boucher L, Breitkreutz A, Tyers M: **BioGRID: a general repository for interaction datasets.** *Nucleic Acids Res* 2006, **34**(Database issue):D535-9.
 53. Ideker TE, Thorsson V, Karp RM: **Discovery of regulatory interactions through perturbation: inference and experimental design.** *Pac Symp Biocomput* 2000:305-316.
 54. Shannon P, Markiel A, Ozier O, Baliga NS, Wang JT, Ramage D, Amin N, Schwikowski B, Ideker T: **Cytoscape: a software environment for integrated models of biomolecular interaction networks.** *Genome Res* 2003, **13**(11):2498-2504.

Publish with **BioMed Central** and every scientist can read your work free of charge

"BioMed Central will be the most significant development for disseminating the results of biomedical research in our lifetime."

Sir Paul Nurse, Cancer Research UK

Your research papers will be:

- available free of charge to the entire biomedical community
- peer reviewed and published immediately upon acceptance
- cited in PubMed and archived on PubMed Central
- yours — you keep the copyright

Submit your manuscript here:
http://www.biomedcentral.com/info/publishing_adv.asp

